

DIRECT SIMULATION CALCULATIONS OF THE RAREFIED HYPERSONIC FLOW PAST A BACKWARD-FACING STEP

Paulo H. M. Leite, phmineiro@lcp.inpe.br

Wilson F. N. Santos, wilson@lcp.inpe.br

National Institute for Space Research, Combustion and Propulsion Laboratory, Cachoeira Paulista-SP, 12630-000 BRAZIL

Abstract. *This work deals with a numerical study on backward-facing steps situated in a rarefied hypersonic flow. The work is motivated by the interest in investigating the step height on the flowfield structure. The primary aim of this paper is to examine the sensitivity of the velocity, density, pressure and temperature due to step-height variations of such backward-facing steps. Effects on the flowfield structure due to variations on the step height have been investigated by employing the Direct Simulation Monte Carlo (DSMC) method. The analysis showed that the flow past a backward-facing step in hypersonic flow is characterized by a strong expansion around de corner of the step, which influences the downstream separation region. It was found that the recirculation region behind of the steps is a function of the rear-face height. The analysis also showed that changing the height of the step did not affect the flow upstream of it. However, disturbances downstream the step depend on changes in the rear-face height of the steps.*

Keywords: *Hypersonic Flow, Rarefied Flow, DSMC, Backward-Facing Step.*

1. INTRODUCTION

A reliable prediction of the thermal and aerodynamics load acting on the vehicle surface is of major importance for the design of a hypersonic vehicle. Contour discontinuities, such as cavities, gaps and/or steps are usually present in the surface, even though a smooth aerodynamic shape of the surface is attempted in the design. Such surface discontinuities may constitute in a potential source in a heat flux rise to the surface or even though in a premature transition from laminar to turbulent flow.

For the particular case of steps, many experimental and theoretical studies (Charwat et al., 1961, Donaldson, 1967, Gai et al., 1989, Gai and Milthorpe, 1995, Grotowsky and Ballmann, 2000, Loth et al., 1992, Rom and Seginer, 1964, Scherberg and Smith, 1967, Shang and Korkegi, 1968) have been conducted in order to understand the physical aspects of a hypersonic flow past to this type of discontinuities, characterized by a sudden change on the surface slope. For the purpose of this introduction, it will be sufficient to describe only a few of these studies.

Data presented by Charwat et al. (1961) indicated that flow which separates from an isolated rearward-facing step impinges on the wall approximately a distance of seven times the step height downstream of the step if the boundary layer is laminar, and approximately five times the step height downstream for a turbulent boundary layer.

Gai and Milthorpe (1995) presented experimental and computational results of a high-enthalpy flow over a blunted-stepped cone. Basically, an axisymmetric rearward-facing step of height of 0.15 and 0.3 times the nose radius of the cone. The analysis showed that the heat transfer rate is typical of that in separated flow, i.e., a sudden fall in heat transfer very near the step and then a gradual increase. The experimental data showed a decrease in heat transfer after reattachment, whereas the numerical prediction exhibited a plateau for a considerable distance.

Grotowsky and Ballmann (2000) investigated laminar hypersonic flow over forward- and backward-facing steps by employing Navier-Stokes equations. The hypersonic flow over the steps were simulated by considering freestream Mach number of 8, Reynolds number of the order of 10^8 and an altitude of 30 km. According to the them, the computational results presented a good agreement with the experimental data available in the literature. They also pointed out that the quantitative comparison exhibited major differences for the wall heat flux, probably due to the difficult in how to measure accurately.

In general, the major interest in these studies has gone into considering laminar or turbulent flow in the continuum flow regime. Nevertheless, there is little understanding of the physical aspects of a hypersonic flow past to steps related to the severe aerothermodynamic environment associated to a reentry vehicle. In this fashion, the purpose of the present account is to investigate the flowfield structure of a hypersonic flow on a backward-facing step in the transition flow regime, i.e., between the continuum flow and the free collision flow regime. Therefore, the focus of the present study is the low-density region in the upper atmosphere, where numerical gaskinetic procedures are available to simulate hypersonic flows. High-speed flows under low-density conditions deviate from a perfect gas behavior because of the excitation of rotational and vibrational modes. At high altitudes, and therefore, low density, the molecular collision rate is low and the energy exchange occurs under non-equilibrium conditions. In such a circumstance, the degree of molecular non-equilibrium is such that the Navier-Stokes equations are inappropriate. Consequently, the Direct Simulation Monte Carlo (DSMC) method will be employed to calculate the hypersonic two-dimensional flow on a backward-facing step.

2. GEOMETRY DEFINITION

In the present account, the imperfections or distortions present on the surface of a reentry capsule is modeled by a backward-facing step. By considering that the rear face h is much smaller than the nose radius R of a reentry capsule, i.e., $h/R \ll 1$, then, the hypersonic flow over the step may be considered as a hypersonic flow over a flat plate with a backward-facing step. Figure 1(a) displays a schematic view of the model employed and presents the important geometric parameters.

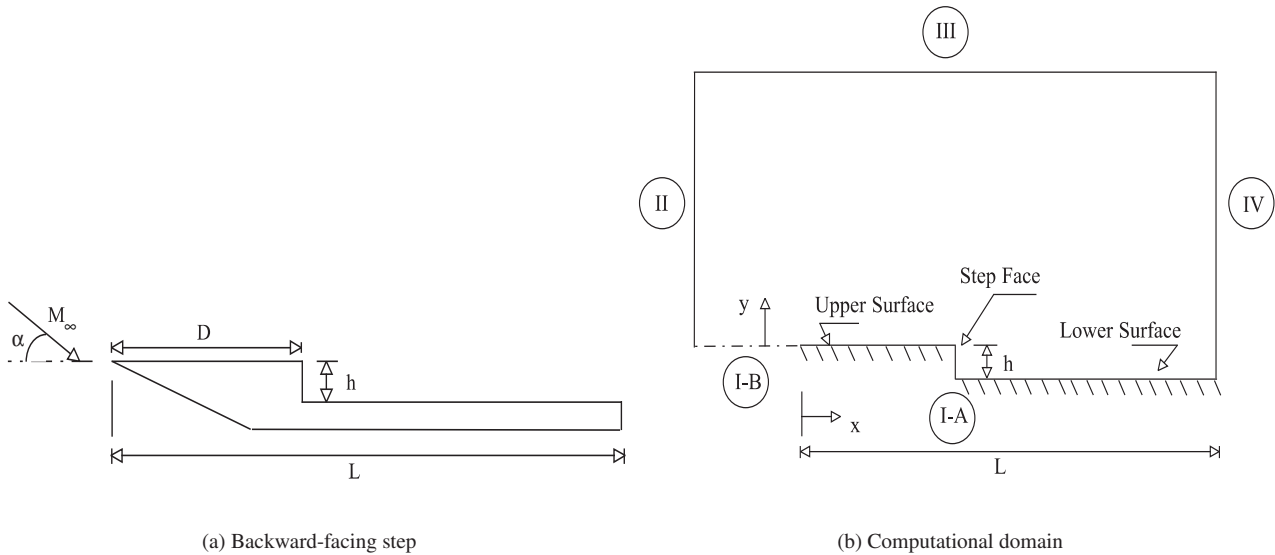


Figure 1. Drawing illustrating (a) the backward-facing step and (b) the computational domain.

According to Fig. 1(a), M_∞ represents the freestream Mach number, α the angle of attack, h the step height, D the location of the step, and L the total length of the flat plate model. The distance D may be understood as being the distance from the stagnation point of the capsule to the step position on the capsule surface. It was considered that the flat plate is infinitely long but only the length L is considered. It was assumed a back step with height h of 3, 6 and 9 mm located $50\lambda_\infty$ downstream of the sharp leading edge. Downstream of the step, the flat plate was extended by $150\lambda_\infty$, where λ_∞ is the freestream mean free path. Therefore, it means that $D/\lambda_\infty = 50$ and $L/\lambda_\infty = 200$.

An understanding of the step height impact on the flowfield structure can be gained by comparing the flowfield behavior of a flat plate with a step to that of a plate without a step. In this fashion, a flat plate free of imperfections, i.e, without steps works as a benchmark for the cases with steps.

3. COMPUTATIONAL METHOD AND PROCEDURE

The Direct Simulation Monte Carlo (DSMC) method, pioneered by Bird (1994), has proved to be the most efficient technique for computing flowfields in which rarefaction effects play a significant role. The method has been tested in the transition flow regime in the last 40 years, and has shown excellent results when compared with experimental data (Harvey, 1986, 2000 and 2003, Holden and Wadhams, 2003).

In the DSMC method, the gas is modeled at the microscopic level by using simulated particles, which each one represents a very large number of physical molecules or atoms. These representative molecules are tracked as they move, collide and undergo boundary interactions in simulated physical space. The molecular motion, which is considered to be deterministic, and the intermolecular collisions, which are considered to be stochastic, are uncoupled over the small time step used to advance the simulation and computed sequentially. The simulation is always calculated as unsteady flow. However, a steady flow solution is obtained as the large time state of the simulation.

Collisions in the present DSMC code are simulated with the variable hard sphere (VHS) molecular model (Bird, 1981) and the no time counter (NTC) collision sampling technique (Bird, 1989). Energy exchange between kinetic and internal modes is controlled by the Borgnakke-Larsen statistical model (Borgnakke and Larsen, 1975). For the present account, the simulations are performed using a non-reacting gas model, consisting of 76.3% of N_2 and 23.7% of O_2 , while considering energy exchange between translational, rotational and vibrational modes. For a given collision, the probability is defined by the inverse of the number of relaxation, which corresponds to the number of collisions needed, on average, for a molecule undergoes relaxation. The probability of an inelastic collision determines the rate at which energy is transferred between the translational and internal modes after an inelastic collision. Relaxation collision numbers of 5 and 50 were

used for the calculations of rotation and vibration, respectively.

For the numerical treatment of the problem, the flowfield around the backward-facing step is divided into an arbitrary number of regions, which are subdivided into computational cells. The cells are further subdivided into subcells, two subcells/cell in each coordinate direction. The cell provides a convenient reference for the sampling of the macroscopic gas properties, while the collision partners are selected from the same subcell for the establishment of the collision rate. The computational domain used for the calculation is made large enough so that body disturbances do not reach the upstream and side boundaries, where freestream conditions are specified. A schematic view of the computational domain is demonstrated in Fig. 1(b). According to this figure, side I-A is defined by the body surface. Diffuse reflection with complete thermal accommodation is the condition applied to this side. In a diffuse reflection, the molecules are reflected equally in all directions, and the final velocity of the molecules is randomly assigned according to a half-range Maxwellian distribution determined by the wall temperature. Side I-B is a plane of symmetry, where all flow gradients normal to the plane are zero. At the molecular level, this plane is equivalent to a specular reflecting boundary. Sides II and III are the freestream side through which simulated molecules enter and exit. Finally, the flow at the downstream outflow boundary, side IV, is predominantly supersonic and vacuum condition is specified (Bird, 1994). At this boundary, simulated molecules can only exit.

The numerical accuracy in DSMC method depends on the cell size chosen, on the time step as well as on the number of particles per computational cell. In the DSMC code, the linear dimensions of the cells should be small in comparison with the scale length of the macroscopic flow gradients normal to the streamwise directions, which means that the cell dimensions should be of the order of or smaller than the local mean free path (Alexander et al., 1998, Alexander et al., 2000). The time step should be chosen to be sufficiently small in comparison with the local mean collision time (Garcia and Wagner, 2000, and Hadjiconstantinou, 2000). In general, the total simulation time, discretized into time steps, is identified with the physical time of the real flow. Finally, the number of simulated particles has to be large enough to make statistical correlations between particles insignificant. These effects were investigated in order to determine the number of cells and the number of particles required to achieve grid independence solutions. Grid independence was tested by running the calculations with half and double the number of cells in the coordinate directions compared to a standard grid. Solutions (not shown) were near identical for all grids used and were considered fully grid independent.

4. FREESTREAM AND FLOW CONDITIONS

The flow conditions represent those experienced by a capsule at an altitude of 70 km. This altitude is associated with the transitional flow regime, which is characterized by the overall Knudsen number of the order of or larger than 10^{-2} . In this manner, the freestream conditions employed in the present calculations are those given by Leite and Santos (2009) and listed in Tab. 1, and the gas properties (Bird, 1994) considered in the simulation are shown in Tab. 2.

Table 1. Freestream flow conditions

Altitude (km)	T_∞ (K)	p_∞ (N/m ²)	ρ_∞ (kg/m ³)	μ_∞ (Ns/m ²)	n_∞ (m ⁻³)	λ_∞ (m)
70	219.69	5.582	8.753×10^{-5}	1.455×10^{-5}	1.8192×10^{21}	9.285×10^{-4}

The freestream velocity U_∞ is assumed to be constant at 7456 m/s, which corresponds to a freestream Mach number M_∞ of 25. The wall temperature T_w is assumed constant at 880 K. This temperature is chosen to be representative of the surface temperature near the stagnation point of a reentry capsule and is assumed to be uniform over the backward-facing step. It is important to mention that the surface temperature is low compared to the stagnation temperature of the air. This assumption seems reasonable since practical surface material will probably be destroyed if surface temperature is allowed to approach the stagnation temperature.

By assuming the rear-face height h as the characteristic length, the Knudsen number Kn_h corresponds to 0.3095, 0.1548 and 0.1032 for height h of 3, 6 and 9 mm, respectively. Finally, the Reynolds number Re_h , also based on the rear-face height h and on conditions in the undisturbed stream, is around 136, 272, and 409 for height h of 3, 6 and 9 mm, respectively.

Table 2. Gas properties

	X	m (kg)	d (m)	ω
O_2	0.237	5.312×10^{-26}	4.01×10^{-10}	0.77
N_2	0.763	4.650×10^{-26}	4.11×10^{-10}	0.74

5. COMPUTATIONAL RESULTS AND DISCUSSION

The purpose of this section is to discuss and to compare differences in the flowfield properties due to variations on the height of the backward-facing step. The flowfield properties of particular interest in this work are velocity, density, pressure and temperature.

5.1 Velocity field

In the DSMC method, the macroscopic properties are computed as averages from the microscopic properties of the molecules in each cell in the computational domain. In this way, the velocity vector is given by the following expression,

$$\mathbf{c}_0 = \frac{\sum_{j=1}^N (m\mathbf{c})_j}{\sum_{j=1}^N m_j} \quad (1)$$

where N , m and \mathbf{c} represent, respectively, the number of molecules, the mass and the velocity vector of the molecules in each cell. It should be noted that the mean molecular velocity $\bar{\mathbf{c}} (\equiv \mathbf{c}_0 = u\vec{i} + v\vec{j} + w\vec{k})$ defines the macroscopic mean velocity. It is important to mention that the velocity of the molecule relative to the mean macroscopic velocity, defined as thermal or peculiar velocity, is denoted by $\mathbf{c}' \equiv \mathbf{c} - \mathbf{c}_0$.

The distribution of tangential velocity u/U_∞ to three sections along the upper surface is illustrated in Fig. 2 as a function of the step height h . In this set of plots, X represents the distance x normalized by the freestream mean free path λ_∞ , and Y the distance y above the upper surface also normalized by λ_∞ . As a basis of comparison, the velocity profiles for the flat plate are illustrated in the same set of plots.

According to Fig. 2, no upstream disturbance is observed on the upper surface in the velocity profiles, i.e., no effect of the presence of the back step is observed. The velocity profiles are identical to those for the flat plate, even for the section at the vicinity of the step, $X = 48$. It is important to mention that the steps are placed at section $X = 50$. Another peculiarity of the flow is with respect to the tangential velocity for $Y \approx 0$, i.e., the velocity along the flat-plate surface and along the upper surface of the step. It is clearly seen that $u/U_\infty \neq 0$ for $Y \approx 0$, a characteristic of a rarefied flow. As a result, the condition of $u/U_\infty = 0$ at the body surface, no-slip velocity in the continuum flow regime, is not applied in rarefied flow.

The distribution of tangential velocity along the lower surface downstream the back step is displayed in Fig. 3 for sections X of 51, 55 and 100. In this set of graphs, Y' is the distance $y + h$ above the lower surface also normalized by λ_∞ . It is clearly seen in this set of graphs that the velocity profiles downstream the back step depend on the step height h . It is observed that the velocity profile is affected more downstream with increasing the step height h . As a result, by increasing the Reynolds number Re_h , the downstream disturbance increases, as would be expected. In addition to that, at the vicinity of the back step, the velocity becomes negative, indicating a recirculation region. Furthermore, far from the back step, at section $X = 100$, the velocity profiles approach the flat-plate velocity profile.

In order to emphasize important features in the flowfield structure, streamline traces at the vicinity of the steps are demonstrated in Fig. 4. In this group of diagrams, Y'_h stands for the vertical distance $y + h$ normalized by the step height h , and X'_h refers to the horizontal distance $x - D$ also normalized by the step height h . In this context, the reference

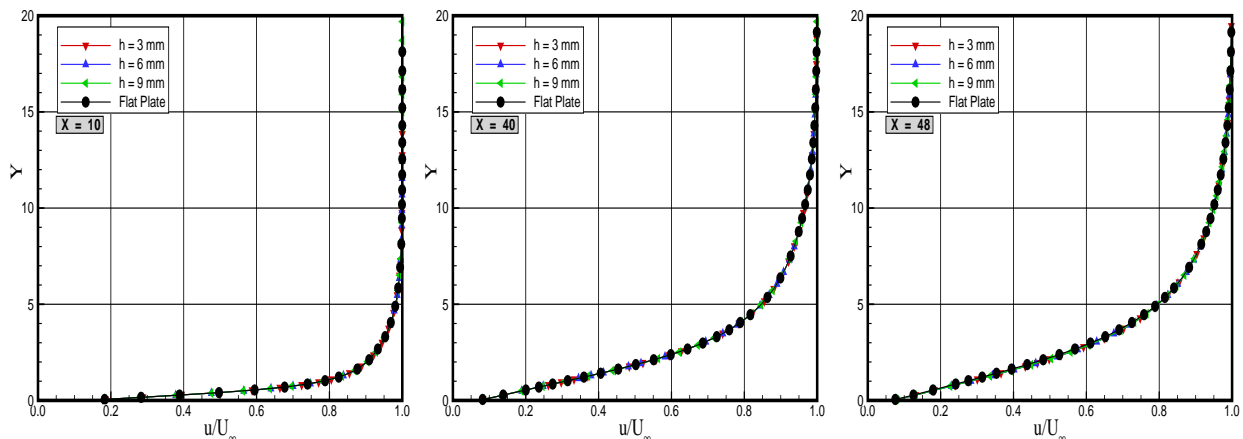


Figure 2. Distribution of tangential velocity (u/U_∞) profiles along the upper surface of the backward-facing step as function of the height h .

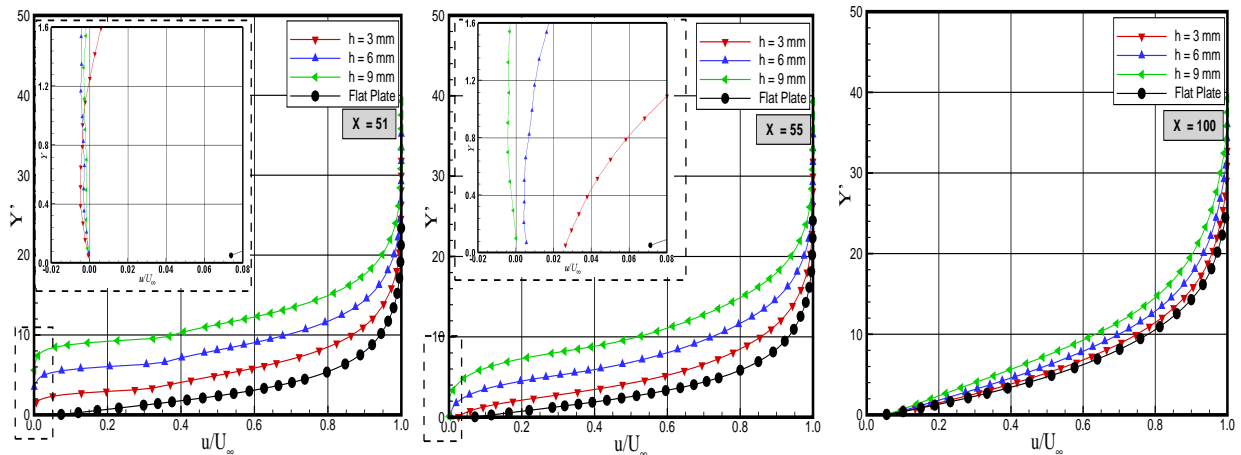


Figure 3. Distribution of tangential velocity (u/U_∞) profiles along the lower surface of the backward-facing step as function of the height h .

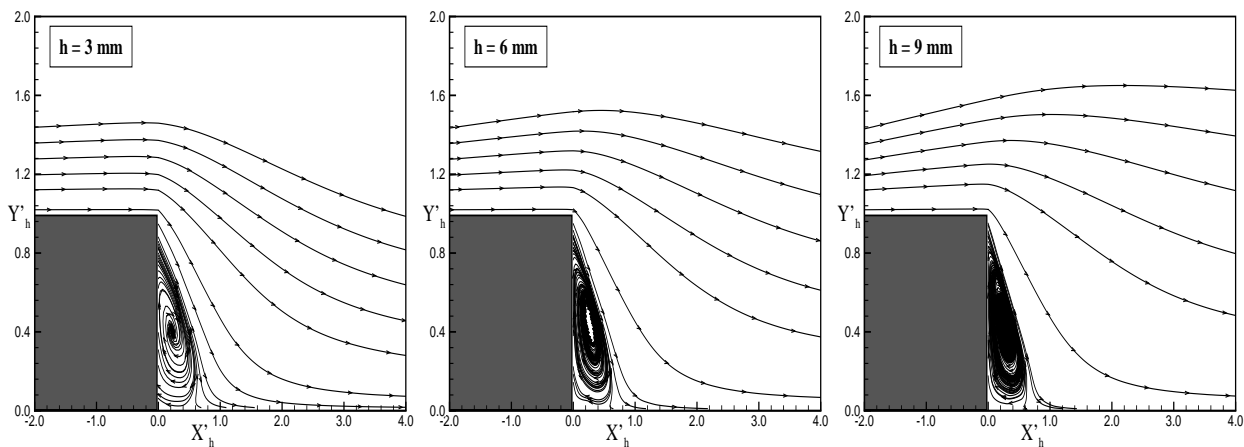


Figure 4. Distribution of streamline traces at the vicinity of the backward-facing step with height h of 3 mm (left), 6 mm (middle) and 9 mm (right).

system shown in Fig. 1(b) was moved to the step position. According to Fig. 4, it is clearly noticed that, for the conditions investigated in the present account, the flowfield experiences an expansion around the corner of the back step and forms a recirculation region at the vicinity of the rear face of the steps. After that, the flowfield is reattached downstream along the lower surface. It is also observed that the recirculation region slightly increases with increasing the rear-face height h or with the Reynolds number Re_h . The reattachment point, x_r , is obtained by assuming that $\tau_w = 0$, i.e., the section on the lower surface where the shear stress is equal to zero. As a result, based on the reference system shown in Fig. 4, X'_{rh} is around 0.16, 0.19 and 0.25 for step height h of 3, 6, and 9 mm, respectively. It is important to mention that X'_{rh} stands for the length $x_r - D$ normalized by the height h . It should be remarked that, after flow reattachment on the lower surface, there is no evidence of the presence of a shock wave, for the conditions investigated. This is in contrast to the flowfield behavior in the continuum flow regime. Usually, in the continuum flow regime, after the flow reattachment, a shock wave formation is observed.

5.2 Density field

The density in each cell in the computational domain is obtained by the following expression,

$$\rho = \frac{1}{V_c} \sum_{j=1}^N m_j \quad (8)$$

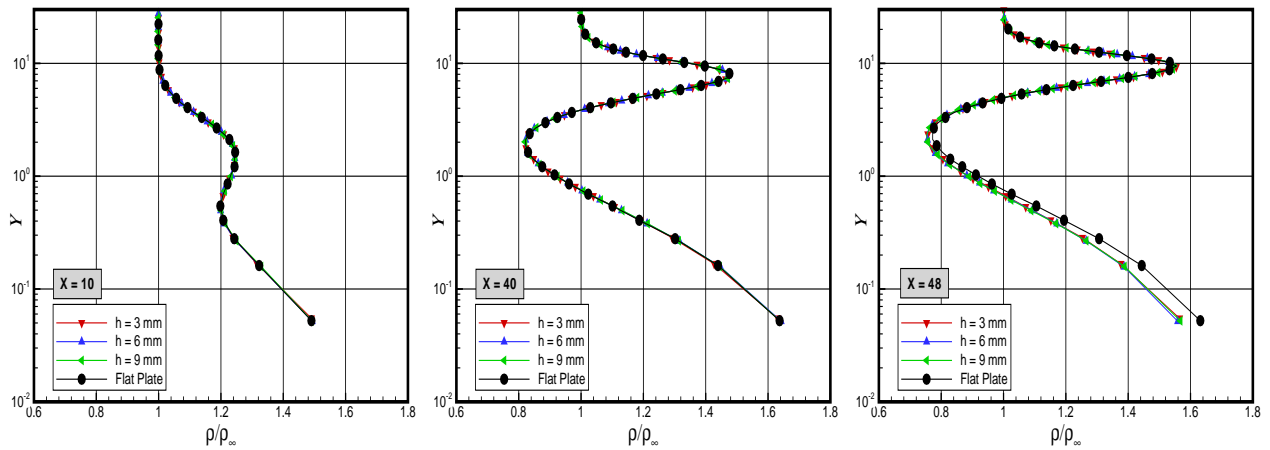


Figure 5. Distribution of density ratio (ρ/ρ_∞) profiles along the upper surface of the backward-facing step as a function of the height h .

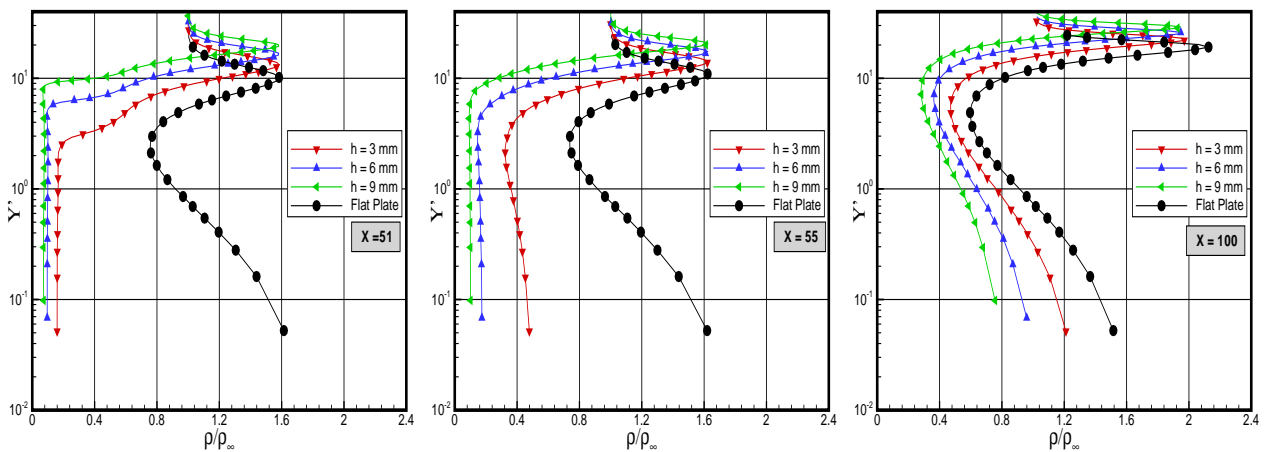


Figure 6. Distribution of density ratio (ρ/ρ_∞) profiles along the lower surface of the backward-facing step as a function of the height h .

where N is the number of molecules in the cell, m is the mass of the molecules and V_c is the volume of the cell.

The distribution of density profiles ρ/ρ_∞ for three sections along the upper surface of the step is displayed in Fig. 5 as a function of the step height h . Similar to the distribution of tangential velocity, the distribution of density profiles is shown in this set of plots to three sections defined by $X = 10, 40$ and 48 . Again X represents the distance x normalized by the freestream mean free path λ_∞ , and Y the distance y above the upper surface also normalized by λ_∞ . As a basis of comparison, density profiles for the flat-plate case are also presented in the same plots.

According to Fig. 5, it is observed that, for sections far from the back steps, density profiles follow the same behavior as that presented for the flat plate, indicating that the flow upstream the back steps has no idea about the presence of the back steps. Nevertheless, close to the step corner, $48 \leq X < 50$, the presence of the steps is slightly felt by the density profiles.

Still referring to Fig. 5, it is apparent that the density ratio shows significant changes in the direction perpendicular to the upper surface of the step. In the Y -direction, the density has a great value when compared to the freestream density. As Y increases from zero, density decreases very fast within a layer of the order of a molecular mean free path λ_∞ . In the following, by increasing Y , density increases further due to the shock wave, and finally decreases again reaching the value of the freestream density, for large values of Y . This behavior is usually observed when the temperature of the body surface is much lower than the stagnation temperature of the gas from the freestream. As a result, the gas near the wall tends to be very cold and denser than the rest of the gas in the boundary layer. For this particular investigation, the ratio of wall temperature to the freestream stagnation temperature is around 0.032.

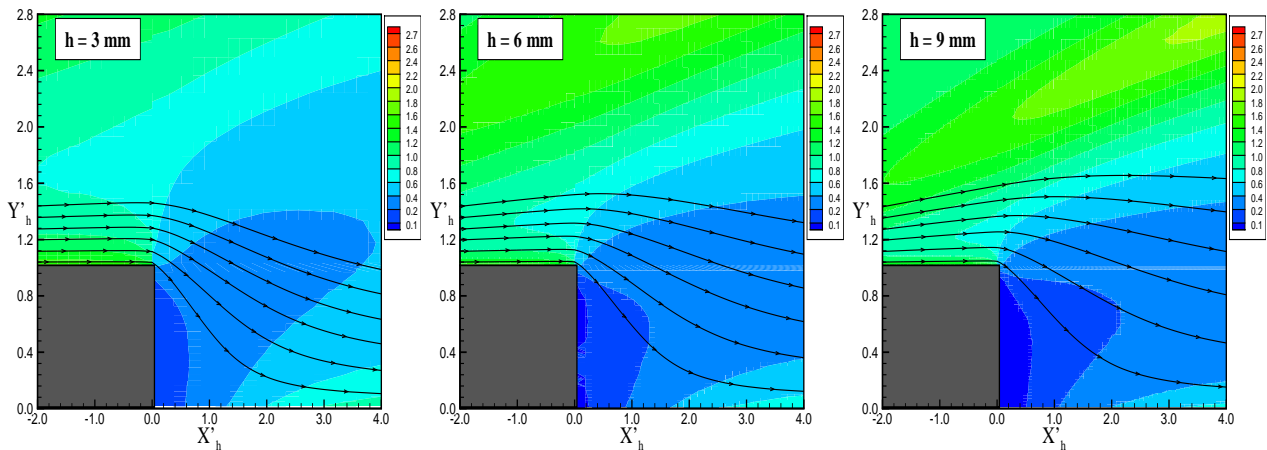


Figure 7. Density ratio (ρ/ρ_∞) contours at the vicinity of the backward-facing step with height h of 3 mm (left), 6 mm (middle) e 9 mm (right).

Density ratio profiles along the lower surface are demonstrated in Fig. 6 for sections X of 51, 55 and 100. Again, for comparison purpose, density profiles for the flat-plate case are also presented in the same figure. It may be recognized from this figure that density profiles are affected by the presence of the steps. As expected, due to the flow expansion, density ρ dramatically decreases as compared to the freestream density ρ_∞ at the vicinity of the back steps. It is also seen that, far from the back steps, $X = 100$, the density profiles seems to approach the flat-plate density profile. It means that, after flow reattachment, the flow behaves like a flow on a flat plate.

In what follows, density ratio contours at the vicinity of the steps are displayed in Fig. 7. In this set of diagrams, Y'_h stands for the vertical distance $y + h$ normalized by the step height h , and X'_h refers to the horizontal distance $x - D$ also normalized by the step height h .

5.3 Pressure field

The pressure in each cell inside de computational domain is obtained by the following equation,

$$p = \frac{1}{3V_c} \sum_{j=1}^N \frac{(mc^2)_j}{N} \quad (3)$$

where N is the number of molecules in the cell, m is the mass of the molecules and V_c is the volume of the cell and c is the velocity of the molecules.

The distribution of pressure ratio p/p_∞ profiles for three sections along the upper surface of the steps is illustrated in Fig. 8 as function of the step height h . In this group of plots, the pressure profiles are shown to three sections defined by $X = 10, 40$ and 48 . According to Fig. 8, it is seen that the pressure profiles follow a similar behavior as those presented by the density profiles. As expected, the pressure profile for the step cases are identical to those obtained for the flat-plate case up to very close to the step corner. It is also seen that, adjacent to the body surface, the pressure p increased one order of magnitude as compared to the freestream pressure p_∞ .

Figure 9 demonstrates the pressure ratio p/p_∞ profiles for three sections along the lower surface of the steps. It is observed that the pressure distribution along the lower surface has similar characteristics as compared to those presented by the density distribution. The pressure ratio presents great changes not only as the flow develops along the lower surface but also along the direction perpendicular to the lower surface. At section $X = 51$, which corresponds to the vicinity of the rear-face of the steps, the pressure is of the order of the freestream pressure p_∞ close to the body surface, i.e., for $Y'_h \simeq 0$. After that, in the direction perpendicular to the low surface, this level of pressure continues constant inside the recirculation region and close to the step corner, $Y'_h = 1$. Afterwards, The pressure ratio increases inside the shock wave and reaches a pick value above 20 times the freestream pressure p_∞ . Along the lower surface, the pressure ratio adjacent to the wall increases and probably will reach the flat-plate profile far from the back step.

In a effort to highlight points of interest, pressure ratio p/p_∞ contours at the vicinity of the steps are illustrated in Fig. 10. In this set of plots, Y'_h represents the length $y + h$ normalized by the step height h , and X'_h refers to distance $x - D$ also normalized by the step height h .

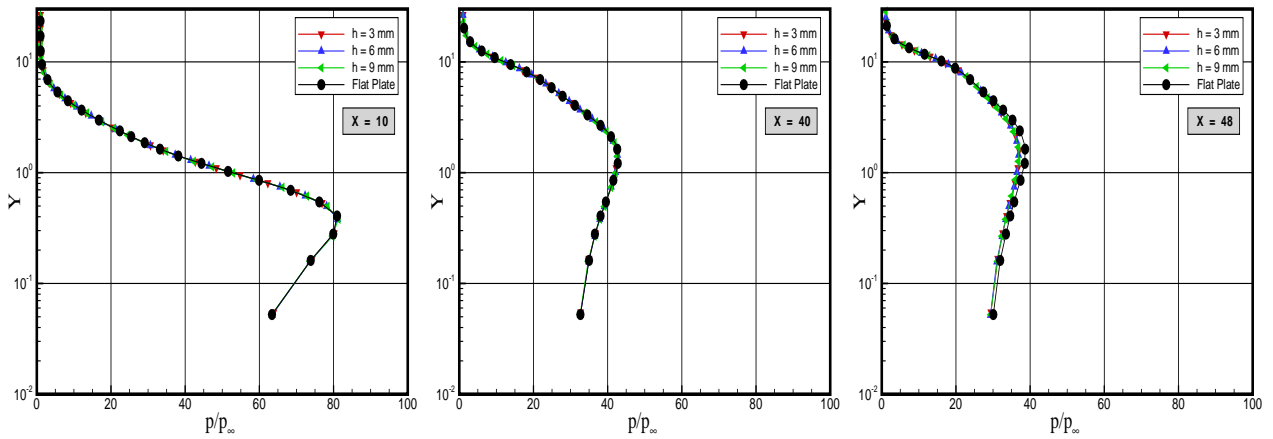


Figure 8. Distribution of pressure ratio (p/p_∞) profiles along the upper surface of the backward-facing step as a function of the height h

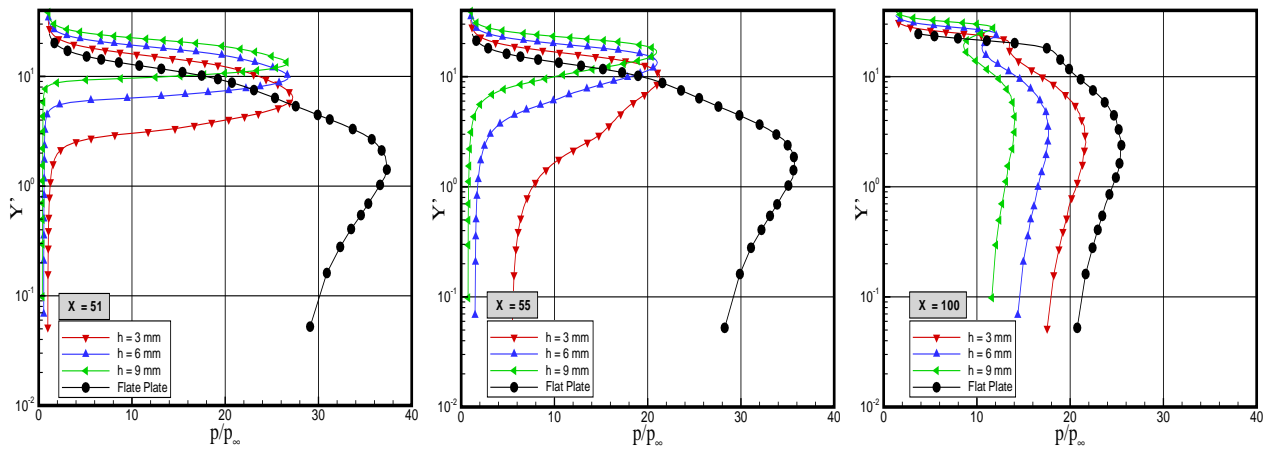


Figure 9. Distribution of pressure ratio (p/p_∞) profiles along the lower surface of the backward-facing step as a function of the height h

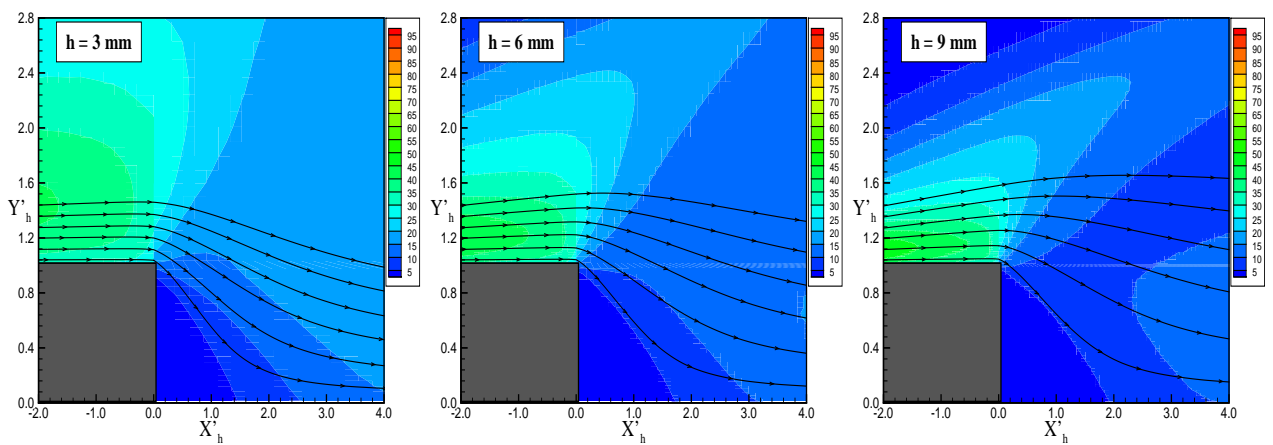


Figure 10. Pressure ratio (p/p_∞) contours at the vicinity of the backward-facing step with height h of 3 mm (left), 6 mm (middle) e 9 mm (right).

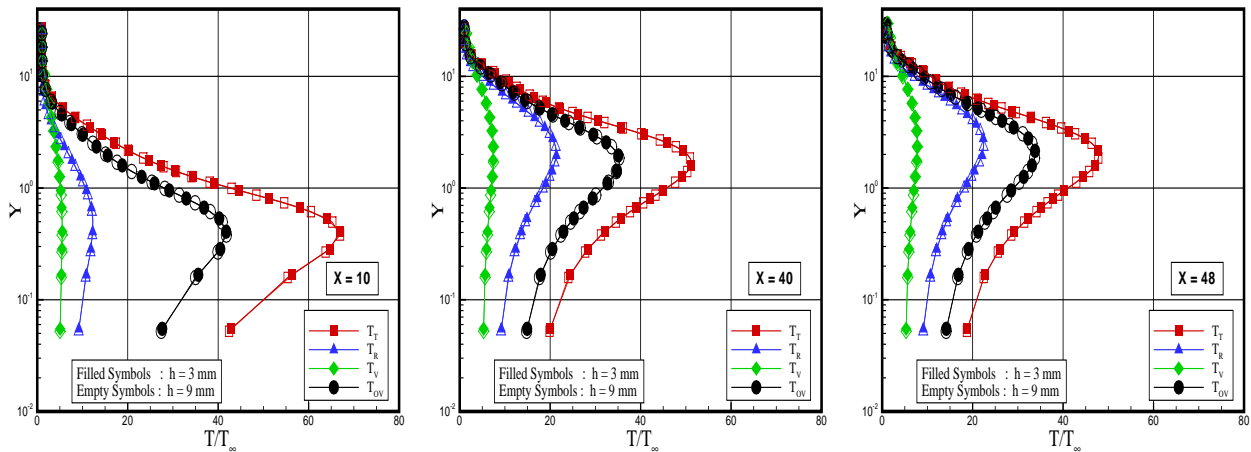


Figure 11. Distribution of kinetic temperature ratio (T/T_∞) profiles along the upper surface of the backward-facing step as a function of the height h .

5.4 Kinetic temperature field

The strong shock wave that forms around the flat plate with a backward-face step at hypersonic flow converts part of the kinetic energy of the freestream air molecules into thermal energy. This thermal energy downstream of the shock wave is partitioned into increasing the translational kinetic energy of the air molecules, and into exciting other molecular energy states such as rotation and vibration.

Temperature ratio profiles along the upper surface are displayed in Fig. 11 for sections X of 10, 40 and 48. In this set of diagrams, temperature ratio stands for the translational temperature T_T , rotational temperature T_R , vibrational temperature T_V or overall temperature T_{OV} normalized by the freestream temperature T_∞ . Also, filled and empty symbols correspond to temperature distributions for rear-face height h of 3 and 9 mm, respectively. It is apparent from these diagrams that thermodynamic non-equilibrium occurs throughout the shock layer, as shown by the lack of equilibrium of the translational and internal kinetic temperatures. Thermal non-equilibrium occurs when the temperatures associated with translational, rotational, and vibrational modes of a polyatomic gas are different. In such a context, it proves convenient to define the overall kinetic temperature. The overall kinetic temperature shown is defined (Bird, 1994) for a non-equilibrium gas as the weighted mean of the translational and internal temperature as follows,

$$T_{OV} = \frac{3T_T + \zeta_R T_R + \zeta_V T_V}{3 + \zeta_R + \zeta_V} \quad (4)$$

where ζ is the degree of freedom and subscript T , R and V stand for translation, rotation and vibration, respectively. The overall kinetic temperature is equivalent to the thermodynamic temperature only in thermal equilibrium conditions. As a matter of fact, it should be noticed that the ideal gas equation of state does not apply to this temperature in a non-equilibrium situation.

Referring to Fig. 11 it is clearly seen that the existence of a downstream back step do not affect the flowfield structure along the upper surface, except for a region very close to the rear-face position. By considering the freestream flow conditions, a freestream Mach number of 25, this result is not a surprise. Of particular interest is the behavior of the temperature close to the surface. According to the prescribed conditions, the wall temperature was set around four times the freestream temperature, i.e., $T_w/T_\infty = 4$. Therefore, the ratio of the overall kinetic temperature to the wall temperature, T_{OV}/T_w , is given by $0.25(T_{OV}/T_\infty)$. With this in mind, it is observed from Fig. 11 that the overall kinetic temperature reaches a value on the upper surface that is above the wall temperature, resulting in a temperature jump as defined in continuum formulation. It is also noticed that the downstream evolution of the flow along the upper surface displays a smearing tendency of the shock wave due to the displacement of the maximum value for the translational temperature as well as for the overall kinetic temperature.

Temperature ratio profiles along the lower surface are illustrated in Fig. 12 for sections X of 51, 55 and 100. In this set of diagrams, Y' is the distance $y + h$ normalized by λ_∞ . According to this set of plots, it is observed that the temperature distribution is a function of the step height h . For the section $X = 51$, therefore very close to the rear face in the recirculation region, the kinetic temperature distribution indicates that temperature is in thermodynamic equilibrium at $Y'_h \simeq 0$, since the temperatures basically attain the same value adjacent to the lower surface. In addition, for the section $X = 100$, therefore far from the rear face as well as the reattachment point, the temperature profiles present basically the

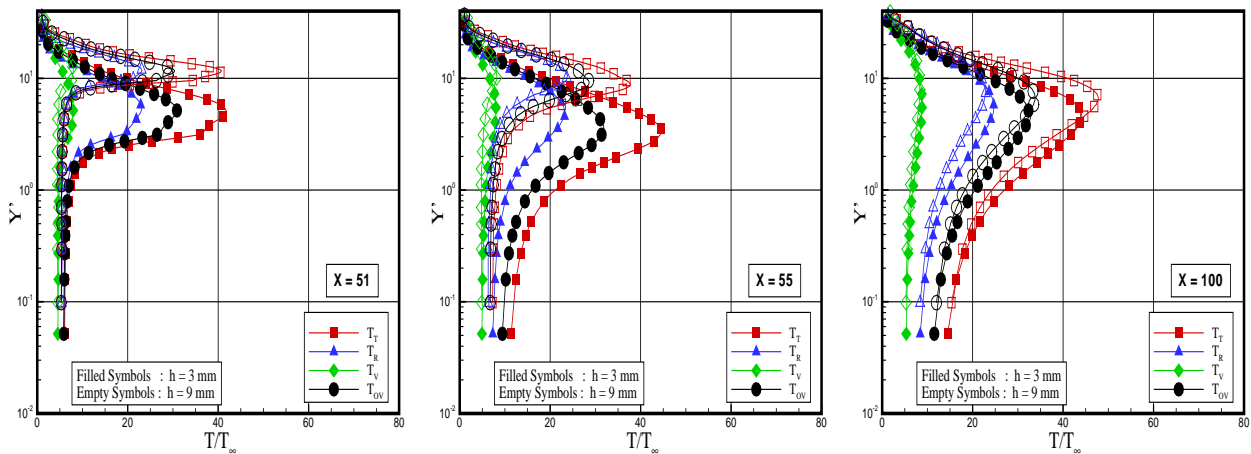


Figure 12. Distribution of kinetic temperature ratio (T/T_∞) profiles along the lower surface of the backward-facing step as a function of the height h .

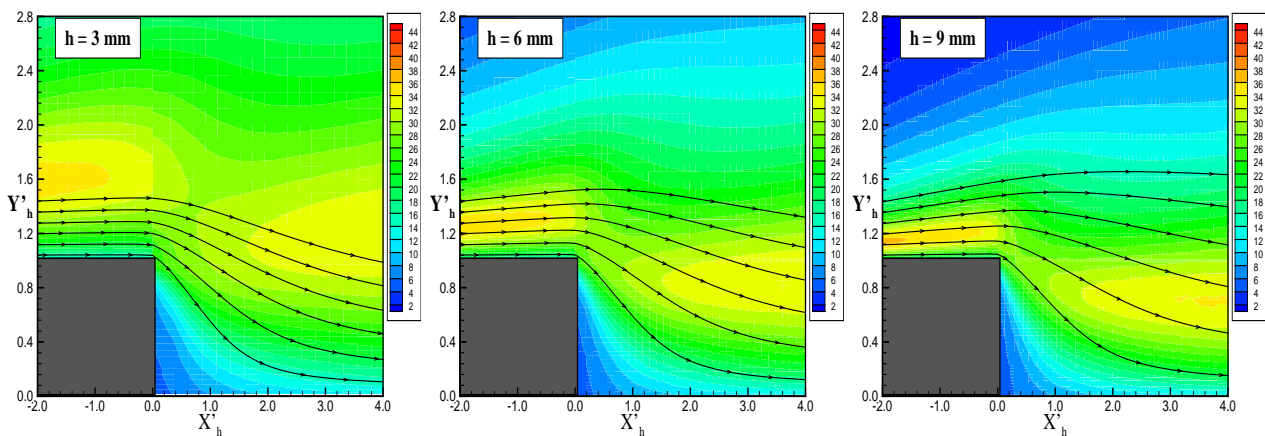


Figure 13. Overall temperature ratio (T_{OV}/T_∞) contours at the vicinity of the backward-facing step with height h of 3 mm (left), 6 mm (middle) e 9 mm (right).

same behavior for the height h investigate.

For comparative purpose, overall temperature ratio T_{OV}/T_∞ contours at the vicinity of the steps are displayed in Fig. 12. Again, in this set of diagrams, Y'_h represents the length $y + h$ normalized by the step height h , and X'_h refers to distance $x - D$ also normalized by the step height h .

6. CONCLUDING REMARKS

Computations of a rarefied hypersonic flow on backward-facing steps have been performed by using the Direct Simulation Monte Carlo method. The calculations provided information concerning the nature of the flowfield structure about the primary flow properties at the vicinity of the steps. Effects of the rear-face height on the velocity, density, pressure, and temperature for a representative range of parameters were investigated. The rear-face height ranged from 3 to 9 mm, which corresponded to Knudsen number Kn_h of 0.3095, 0.1548 and 0.1032, respectively. Therefore, in the transition flow regime. The analysis showed that the flow separation takes place on the corner of the step, and the flow reattaches downstream on the lower surface of the step. A recirculation region is formed downstream of the rear-face of the step and the size of the region depends on the rear-face height. Also, it was found that the downstream disturbance due to the presence of the steps increased with increasing the rear-face height. Moreover, the extent of this disturbance depends on the flowfield property.

7. ACKNOWLEDGEMENTS

The authors would like to thank the financial support provided by CNPq (Conselho Nacional de Desenvolvimento Científico e Tecnológico) under Grant No. 473267/2008-0.

8. REFERENCES

- Alexander, F. J., Garcia, A. L., and Alder, B. J., 1998, "Cell Size Dependence of Transport Coefficient in Stochastic Particle Algorithms", *Physics of Fluids*, Vol. 10, No. 6, pp. 1540–1542.
- Alexander, F. J., Garcia, A. L., and Alder, B. J., 2000, "Erratum: Cell Size Dependence of Transport Coefficient is Stochastic Particle Algorithms", *Physics of Fluids*, Vol. 12, No. 3, pp. 731–731.
- Bird, G. A., 1981, "Monte Carlo Simulation in an Engineering Context", *Progress in Astronautics and Aeronautics: Rarefied gas Dynamics*, Ed. Sam S. Fisher, Vol. 74, part I, AIAA New York, pp. 239–255.
- Bird, G. A., 1989, "Perception of Numerical Method in Rarefied Gasdynamics", *Rarefied gas Dynamics: Theoretical and Computational Techniques*, Eds. E. P. Muntz, and D. P. Weaver and D. H. Capbell, Vol. 118, *Progress in Astronautics and Aeronautics*, AIAA, New York, pp. 374–395.
- Bird, G. A., 1994, "Molecular Gas Dynamics and the Direct Simulation of Gas Flows", Oxford University Press, Oxford, England, UK.
- Borgnakke, C. and Larsen, P. S., 1975, "Statistical Collision Model for Monte Carlo Simulation of Polyatomic Gas Mixture", *Journal of Computational Physics*, Vol. 18, No. 4, pp. 405–420.
- Charwat, A. F., Dewey, C. F., Roos, J. N. and Hitz, J. A., 1961, "An Investigation of Separated Flows. 1: The Pressure Field", *Journal of aerospace Sciences*, Vol. 28, No. 6, pp. 457–470.
- Donaldson, I. S., 1967, "On the Separation of a Supersonic Flow at a Sharp Corner", *AIAA Journal*, Vol. 5, No. 6, pp. 1086–1088.
- Gai, S.L., and Milthorpe, J. F., 1995, "Hypersonic High-Enthalpy Flow over a Blunt-Stepped Cone", *Proceedings of the 20th International Symposium on Shock Waves*, pp. 234–244.
- Gai, S. L., Reynolds, C. R., and Baird, J. P., 1989, "Measurements of Heat Transfer in Separated High-Enthalpy Dissociated Laminar Hypersonic Flow Behind a Step", *Journal of Fluid Mechanics*, Vol. 199, pp. 541–561.
- Garcia, A. L., and Wagner, W., 2000, "Time Step Truncation Error in Direct Simulation Monte Carlo", *Physics of Fluids*, Vol. 12, No. 10, pp. 2621–2633.
- Grotowsky, M. G., and Ballmann J., 2000, "Numerical Investigation of Hypersonic Step-Flows", *Shock Waves*, Vol. 10, pp. 57–72.
- Hadjiconstantinou, N. G., 2000, "Analysis of Discretization in the Direct Simulation Monte Carlo", *Physics of Fluids*, Vol. 12, No. 10, pp. 2634–2638
- Harvey, J. K., 1986, "Direct Simulation Monte Carlo Method and Comparison with Experiment", AIAA, Washington, DC.
- Harvey, J. K., 2000, "Review of Code Validation Studies in High-Speed Low-Density Flows", *Journal of Spacecraft and Rockets*, Vol. 37, No. 1, pp. 8–20.
- Harvey, J. K., 2003, "A review of a validation Exercise on the Use of the DSMC Method to Compute Viscous/Inviscid Interactions in Hypersonic Flow", AIAA Paper 2003–3643.
- Holden, M. S. and Wadhams, T. P., 2003, "A review of Experimental Studies for DSMC and Navier-Stokes Code Validation in Laminar Regions of Shock/Shock and Shock/Boundary layer Interaction Including Real Gas Effects in Hypersonic Flows ", AIAA Paper 2003–3641.
- Leite, P. H. M., and Santos, W. F. N., 2009, "Direct Simulation of Low Density Hypersonic Flow over a Forward-Facing Step", 20th International Congress of Mechanical Engineering, COBEM 2009, November 15–20, Gramado, RS, Brazil (Accepted).
- Loth, E., Kailasanath, K., and Löhner, R, 1992, "Supersonic Flow over an Axisymmetric Backward-Facing Step", *Journal of Spacecraft and Rockets*, Vol. 29, No. 3, pp. 352–359.
- Rom, J., and Seginer, A., 1964, "Laminar Heat Transfer to a two-Dimensional Backward Facing Step from the High-Enthalpy Supersonic Flow in the Shock Tube", *AIAA Journal*, Vol. 2, No. 2, pp. 251–255.
- Scherberg, M. G., and Smith, H. E., 1967, "An Experimental Study of Supersonic Flow over a Rearward Facing Step", *AIAA Journal*, Vol. 5, No. 1, pp. 51–56.
- Shang, J. S., and Korkegi, R. H., 1968, "Investiation of Flow Separation over a Rearward-Facing Step in a Hypersonic Stream", *AIAA Journal*, Vol. 6, No. 5, pp. 986–987.

9. Responsibility notice

The authors are the only responsible for the printed material included in this paper.